Shell model study of $N \simeq 28$ neutron-rich nuclei

L. Gaudefroy*
CEA, DAM, DIF, F-91297 Arpajon, France
(Received 15 March 2010; revised manuscript received 10 June 2010; published 30 June 2010)

A systematic study of the low-lying structure of $N = 27$, 28, and 29 isotones is performed within the shell model framework using the SDPF-U interaction [F. Nowacki and A. Poves, Phys. Rev. C **79**, 014310 (2009)]. For each isotonic chain, correlation energy is found to increase while moving away from the stability line. Spherical shapes as well as small values of correlation energy are associated with the isotopes of $_{20}$Ca and $_{19}$K discussed in this study. Neutron intruder states appear at low excitation energy in the $_{18}$Ar and $_{17}$Cl studied isotopes. Coexistence between spherical and prolate deformed states is a systematic feature in $_{16}$S isotopes. Below $Z = 16$ most of the studied nuclei are characterized by intruder ground states. The major role played by protons in determining the structure of $N \simeq 28$ nuclei is shown.

DOI: 10.1103/PhysRevC.81.064329 PACS number(s): 21.60.Cs, 21.10.Hw, 21.10.Jx, 21.10.Ky

I. INTRODUCTION

About 20 years after the β-decay experiment that provided the first hints on the reduction of the $N = 28$ gap in neutron-rich nuclei [1], the study of this mass region is still an active area of research. Taking advantage of the development of radioactive ion beams, numerous experimental data for neutron-rich nuclei with $N \simeq 28$ have been obtained. Coulomb excitation experiments [2–5] confirmed first the onset of collectivity while moving away from the valley of stability. Mass measurements also indicated the reduction of the $N = 28$ gap [6,7], as well as the results from in-beam γ-ray spectroscopy [8–10]. More recently, various nuclei have been studied by means of direct reactions [11–16]. A global analysis of these data shows the reduction of the $N = 28$ shell gap in exotic nuclei. The signature of deformation has been obtained in some of the most recent studies [17–19]. These experimental efforts have been accompanied by simultaneous theoretical developments. Both mean field [20–24] and shell model [25–29] approaches contributed to the cross-fertilization between experiment and theory.

In the case of a shell model approach, the wealth of data obtained within the past 20 years allowed a refinement of the monopole part of the *sdpf* interactions used to describe this mass region. The resulting up-to-date interaction, namely the SDPF-U interaction [30], provides a remarkably good description of available data for nuclei in the vicinity of the $N = 28$ shell closure. This interaction thus offers the opportunity to systematically study nuclei in this mass region in order to gain a deeper understanding of the evolution of nuclear structure and its associated signatures. The present article reports on such a systematic study. The nuclei studied here are denoted by gray boxes in the left panel of Fig. 1. The structure of the other nuclei has already been discussed elsewhere using the same approach and interaction [13,30].

This article is organized as follows. Section II A discusses the impact of correlations on the low-lying structure of odd-odd $N = 27$ isotones. This discussion is complementary to that for even-odd isotones reported in Ref. [13]. Section II B focuses on the structure of low-lying states in odd-even $N = 28$ isotones to clarify the role of proton excitations in the evolution of nuclear structure in this mass region. Section II C1 investigates if and how correlations impact the structure of even-odd $N = 29$ isotones, while Sec. II C2 discusses the structure of odd-odd $N = 29$ isotones. Section III summarizes the picture emerging from the present work and suggests experimental perspectives.

II. DISCUSSION

The results presented in this section are obtained using the ANTOINE code [31,32]. Shell model calculations are performed within the full sd (fp) valence space for protons (neutrons) as shown in the right panel of Fig. 1. Effective charges ($e_\pi = 1.35$ and $e_\nu = 0.35$) and nucleon g-factors ($g_\ell^\pi = 1.1$, $g_s^\pi = 4.1895$, $g_\ell^\nu = -0.1$, and $g_s^\nu = -2.8695$) are used to estimate electromagnetic properties.

In this article the *natural/intruder* terminology refers to neutron configurations. A *natural* neutron configuration refers to a configuration corresponding to the filling of lowest energy for the valence orbitals reported in the right panel of Fig. 1. At $N = 27$, it corresponds to a single hole in the $\nu f_{7/2}$ orbit $[(\nu f_{7/2})^{-1}]$. At $N = 28$, the *natural* configuration corresponds to the $\nu f_{7/2}$ orbit fully occupied $[(\nu f_{7/2})^8]$ and to a single particle in the $\nu p_{3/2}$ orbit at $N = 29$ $[(\nu f_{7/2})^8 (\nu p_{3/2})^1]$. An *intruder* neutron configuration refers to an excited configuration obtained when at least one $\nu f_{7/2}$ neutron from the natural configuration is promoted in higher fp orbits.

For convenience, definitions of monopole and multipole contributions to the total energy of a shell model state are given here (see Refs. [29,33] for further details). The shell model Hamiltonian can be written as $H = H_m + H_M$. The monopole part, H_m, is responsible for global saturation properties and single-particle behavior. It contains contributions of spherical Hartree-Fock type. The multipole Hamiltonian, H_M, contains all other terms, such as pairing and quadrupole correlations. It is responsible for collective behavior. This separation property of H allows us to decompose the total energy of a shell model state, E, into its monopole and multipole contributions, respectively, referred to as MoC and MuC in the

*laurent.gaudefroy@cea.fr

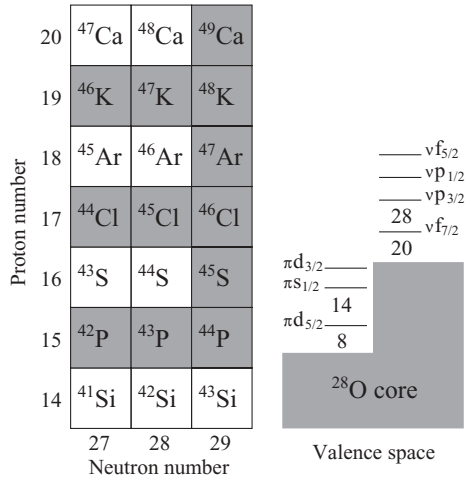

FIG. 1. Left panel: Portion of the nuclear chart being investigated. Nuclei marked by gray boxes are those discussed in the article. Right panel: Schematic view of the valence space used in present shell model calculations. The magic numbers 8, 14, 20, and 28 are reported.

following. Indeed, for a given eigenfunction, $|\Psi\rangle$, of H one has $H|\Psi\rangle = E|\Psi\rangle$, MoC $= \langle\Psi|H_m|\Psi\rangle$, MuC $= \langle\Psi|H_M|\Psi\rangle$, and $E =$ MoC + MuC. This decomposition is intensively used throughout this article.

A. $N = 27$ isotopes

In a naive shell model (SM) picture the ground-state (GS) wave function of $N = 27$ isotones is expected to be dominated by the $(\nu f_{7/2})^{-1}$ neutron configuration, and the $(\nu f_{7/2})^{-2}(\nu p_{3/2})^{+1}$ configuration is expected in the low-lying excitations of these nuclei. This is indeed observed in $^{47}_{20}$Ca$_{27}$, which presents quasipure $7/2^-$ GS and $3/2^-$ first excited state at about 2 MeV. However several experimental studies, complemented by SM calculations, have shown that the structure of low-lying states in $N = 27$ isotones is more complex than suggested previously as soon as one departs from the $Z = 20$ shell closure. Indeed, in $^{45}_{18}$Ar, in-beam γ-ray spectroscopy [9] and direct reactions [11,13] revealed that the wave function describing the $3/2^-_1$ state, lying as low as 550 keV, is a complex mixture of single particlelike and core-excited components (see the corresponding detailed discussion in Ref. [13]).

Available experimental data closer to the neutron drip line show that configuration mixing increases with the N/Z ratio. The ground state of $^{44}_{17}$Cl, studied via a neutron knockout reaction [15] and g-factor measurement [34], contains an almost equivalent part of the natural $(\nu f_{7/2})^{-1}$ and intruder $(\nu f_{7/2})^{-2}(\nu p_{3/2})^{1}$ configurations. In $^{43}_{16}$S, g-factor measurement strongly points toward the intruder nature of the ground state at $Z = 16$, the natural $(\nu f_{7/2})^{-1}$ state lying $\simeq$ 320 keV in excitation energy [19]. These results in ^{43}S have been partly confirmed by Riley and co-workers [16]. Within the shell model framework these spectroscopic data are the result of the progressive reduction of the $N = 28$ shell gap and the increase of correlation energy from stability toward exotic nuclei [13]. The present discussion aims at extending that of Ref. [13] to the odd-odd $N = 27$ isotones to determine the impact of correlations on the low-lying structure in $^{46}_{19}$K, $^{44}_{17}$Cl, and $^{42}_{15}$P.

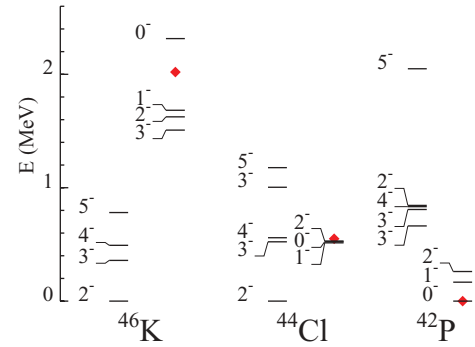

FIG. 2. (Color online) Calculated level schemes in odd-odd $N = 27$ isotones of interest. States originating from the $\pi d_{3/2}$-$\nu f_{7/2}$ and $\pi d_{3/2}$-$\nu p_{3/2}$ couplings are reported. States clearly identified as being built on the latter configuration are shifted on the right part of the level scheme for each isotone. The diamond symbol indicates, for each $^{A}_{Z}X$ isotone, the position of the first $3/2^-$ state in the core nucleus $^{A+1}_{Z+1}Y$.

With a proton number ranging from 15 to 19, the low-lying states of these isotones are expected to be mainly described by the coupling of an unpaired proton in the $(\pi s_{1/2}, \pi d_{3/2})$ degenerate orbits with an unpaired neutron in either the $\nu f_{7/2}$ or the $\nu p_{3/2}$ orbits (see Fig. 1). The calculated level schemes for $^{46}_{19}$K, $^{44}_{17}$Cl, and $^{42}_{15}$P, restricted to states of interest for the present discussion, are shown in Fig. 2. In $^{46}_{19}$K, the $\pi d_{3/2}$-$\nu f_{7/2}$ configuration gives rise to the $(2_1,3_1,4_1,5_1)^-$ multiplet calculated to lie below 1 MeV in good agreement with available data [35,36]. Non-negligible mixing with the $\pi s_{1/2}$-$\nu f_{7/2}$ configuration is found for the 3^-_1 and 4^-_1 states of the multiplet. It is associated with the experimentally well-established degeneracy of the $\pi s_{1/2}$ and $\pi d_{3/2}$ orbits in this mass region [37,38], in agreement with SM calculations [30]. The consequence of the degeneracy of the $s_{1/2}$ and $d_{3/2}$ proton orbits is not discussed in detail in the present article as it has been discussed elsewhere [30,37,38].

The $(0_1,1_1,2_2,3_2)^-$ states built on the $\pi d_{3/2}$-$\nu p_{3/2}$ configuration are calculated to lie around 2 MeV. This excitation energy is consistent with that for the $3/2^-_1$ state in $^{47}_{20}$Ca, built on the $\nu p_{3/2}$ orbit, reported in Fig. 2 (diamond symbol) in the level scheme of $^{46}_{19}$K. In $^{46}_{19}$K, the states of interest present rather pure wave functions (WFs) with about 70% corresponding to the aforementioned neutron configurations. This is exemplified in Fig. 3 which displays the amount of natural and intruder neutron configurations in the ground-state wave functions of the considered $N = 27$ isotones.

As seen from Fig. 2, states built on the $\pi d_{3/2}$-$\nu p_{3/2}$ configuration, in $^{44}_{17}$Cl, are calculated to be about 1.5 MeV lower in excitation energy than those in $^{46}_{19}$K. This result is consistent with the experimentally established lowering of the neutron intruder configuration between $^{47}_{20}$Ca and $^{45}_{18}$Ar [9,11,13] (see Fig. 2). Associated with this lowering, a large mixing between natural and intruder neutron configurations is found in the WFs of the calculated states for $^{44}_{17}$Cl as displayed in Fig. 3 for the particular case of the GS. This result is in agreement with the experimental data reported recently by Riley *et al.* [15] and

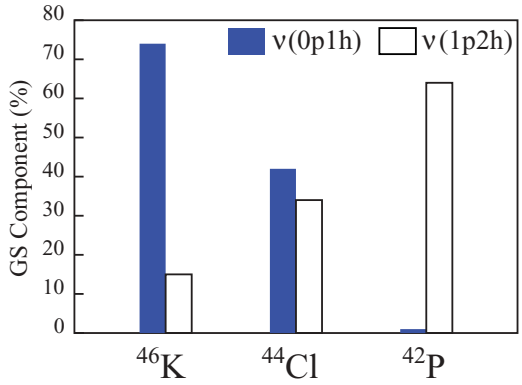

FIG. 3. (Color online) Components of natural (0p1h) and intruder (1p2h) neutron configurations in the ground-state wave function of odd-odd $N = 27$ isotones discussed in the text.

De Rydt *et al.* [34]. The increasing contribution of the intruder component in the WF of the GS of odd-odd $N = 27$ isotones is consistent with the increasing contribution of multipole energy to the total energy of the states of interest. The monopole- and multipole-energy contributions to the total energy of these states are reported in Table I. Interestingly, considering only the monopole contribution (i.e., contribution from the spherical mean field), the ground state of these isotones (in boldface in Table I) is calculated to be part of the natural $\pi d_{3/2}$-$\nu f_{7/2}$ configuration. In $^{44}_{17}$Cl, the states built on the intruder $\pi d_{3/2}$-$\nu p_{3/2}$ configuration are energetically favored as compared to those built on the natural configuration because of a gain in multipole energy of about 2–3 MeV.

Further from the stability line, experimental evidence for the intruder nature of the GS in $^{43}_{16}$S has been reported [19] and accounted for by shell model calculations [13,19]. Consistently, in $^{42}_{15}$P, states built on the $\pi d_{3/2}$-$\nu p_{3/2}$ intruder configuration are calculated as the ground and first excited states, as shown in Fig. 2. The 0^- GS of the nucleus contents only a negligible (<1%) component of the natural $(\nu f_{7/2})^{-1}$ neutron configuration, as displayed in Fig. 3. Similar negligible contributions of natural configurations are found for the first and second excited states shown in Fig. 2. The first state calculated with a non-negligible $(\nu f_{7/2})^{-1}$ natural configuration (49%) is the 3^-_1 state, 675 keV above the intruder ground state. Correlations are found to be responsible for the natural/intruder inversion in $^{42}_{15}$P, as shown in Table I.

TABLE I. Decomposition of the total energy of the states discussed in $N = 27$ isotones in terms of their monopole (MoC) and multipole contributions (MuC), in MeV.

J^π	^{46}K		^{44}Cl		^{42}P	
	MoC	MuC	MoC	MuC	MoC	MuC
0^-_1	−311.4	−6.4	−264.4	−13.5	−217.1	−14.7
1^-_1	−311.8	−6.9	−264.4	−13.5	−216.8	−14.8
2^-_1	−313.6	−4.9	−267.2	−11.3	−216.8	−14.7
2^-_2	−313.9	−6.8	−264.5	−13.4	−216.1	−14.7
3^-_1	−315.0	−3.9	−267.0	−10.9	−213.5	−17.5
3^-_2	−315.4	−4.7	−266.4	−11.0	−213.0	−17.9
4^-_1	−315.8	−4.1	−267.1	−10.8	**−219.0**	−11.9
5^-_1	**−315.9**	−3.8	**−268.3**	−8.9	−213.7	−16.0

The previous discussion on odd-odd $N = 27$ isotones completes consistently that presented in Ref. [13]. Correlations gradually increase while moving toward neutron-rich nuclei along the $N = 27$ isotonic chain. Above $Z = 17$, the ground state of these isotones is mainly built on the natural neutron configuration $[(\nu f_{7/2})^{-1}]$, while equivalent mixing between that configuration and the intruder $[(\nu f_{7/2})^{-2}\,(\nu p_{3/2})^{1}]$ neutron configuration is predicted and observed in $^{44}_{17}$Cl$_{27}$. Below $Z = 17$, the ground states of $N = 27$ isotones are predicted to be neutron intruder states.

B. $N = 28$ isotones

From previous experimental and theoretical studies it appears that the reduction of the $N = 28$ gap in neutron-rich nuclei is no longer a subject of debate [39]. The predicted deformation in $^{42}_{14}$Si$_{28}$ is often presented as an example of the disappearance of the $N = 28$ spherical shell effect. However, no clear conclusion is available concerning the role of protons in the development of collectivity in the vicinity of this nucleus. In the available literature, some authors claim that moderate or important proton excitations from the $\pi d_{5/2}$ orbit are required to explain the experimental spectroscopic results found in S and Si isotopes [13,18,30]. On the contrary, others argue that the reduction of the $N = 28$ shell gap, solely, accounts for the observed spectroscopic properties in this mass region and thus conclude that a large $Z = 14$ shell gap [37,40–43] hinders proton correlations.

The present discussion is devoted to this question. The low-lying structure of odd-even $N = 28$ isotones, with $Z > 14$, offers a unique opportunity to study states built on the proton *sd* orbits and hence to probe the $Z = 14$ shell gap and the role of proton excitations across this latter.

Shell model calculations have been performed for $^{47}_{19}$K, $^{45}_{17}$Cl, and $^{43}_{15}$P to identify states built on the $\pi s_{1/2}$, $\pi d_{3/2}$, and $\pi d_{5/2}$ proton orbits. The resulting level schemes are presented in Fig. 4. The first low-lying states of these isotones are expected to be quasidegenerate in energy being built on the $\pi s_{1/2}$ and $\pi d_{3/2}$ proton orbits (in agreement with present results reported in Fig. 4). States built on the $\pi d_{5/2}$ proton orbit are expected to lie at higher excitation energy, depending on the amount of proton excitation across the $Z = 14$ shell gap. In the following, states built on the $\pi d_{5/2}$ proton orbit are considered to be those with a $5/2^+$ spin and parity and a non-negligible part of their wave function corresponding to a hole in the $\pi d_{5/2}$ proton orbit. In $^{47}_{19}$K, the $5/2^+_6$ state is the first one fulfilling these criteria. It is calculated to lie at 5.5 MeV, as shown in Fig. 4. All other calculated $5/2^+$ states, below 5.5 MeV, are interpreted as recoupled states, as about (or more than) 90% of their proton wave function correspond to the $(\pi d_{5/2})^6$ component. This is, for example, the case for the $5/2^+_1$ and $5/2^+_2$ states represented as gray levels in Fig. 4 at 3.00 and 3.45 MeV, respectively. Their wave functions are dominated by a proton hole in the degenerate $\pi d_{3/2}$ and $\pi s_{1/2}$ orbits coupled with the 2^+_1 state in the core nucleus $^{48}_{20}$Ca (the excitation energy of the 2^+_1 state in $^{48}_{20}$Ca is reported as a diamond symbol in the level scheme of

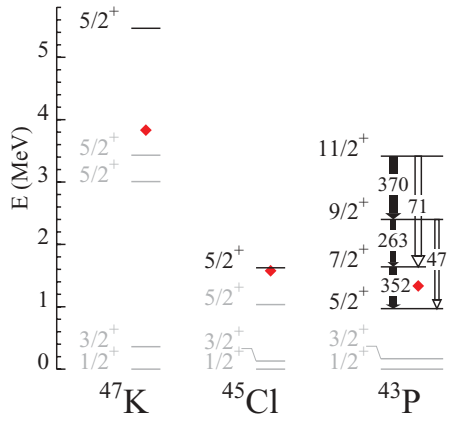

FIG. 4. (Color online) Calculated level schemes for $N = 28$ isotones discussed in the text. Only states of interest are shown (see text for details). Levels identified as being built on the $d_{5/2}$ proton orbit are reported in black. The diamond symbol indicates, for each ${}^{A}_{Z}X$ isotone, the position of the 2^+_1 state in the core nucleus ${}^{A+1}_{Z+1}Y$. $M1$ reduced transition probabilities (in $10^{-3}\mu_N^2$) are denoted by the black arrows. $E2$ reduced transition probabilities (in e^2 fm^4) denoted by the empty arrows.

${}^{47}_{19}$K). For the sake of clarity other $5/2^+$ states are not shown in Fig. 4. The level scheme calculated for ${}^{47}_{19}$K is in good agreement with available data [44]. In particular, a $5/2^+$ state has been reported at 5.4 MeV with a proton spectroscopic factor of about 1 (normalized to 6) indicating that this state exhausts a non-negligible fraction of the $\pi d_{5/2}$ spectroscopic strength. As shown in Ref. [44], the spectroscopic strength for the latter orbit is considerably more fragmented than that for the $\pi s_{1/2}$ and $\pi d_{3/2}$ orbits in ${}^{47}_{19}$K. This is associated with the large binding energy of the $\pi d_{5/2}$ orbit. Similar results are obtained in the present shell model calculations. Figure 5 displays the contribution of the $(\pi d_{5/2})^{-1}$ component to the wave function of the $5/2^+$ states indicated as black levels in Fig. 4. As seen from this figure, only 25% of the wave function of the $5/2^+_6$ state in ${}^{47}_{19}$K corresponds to a hole in

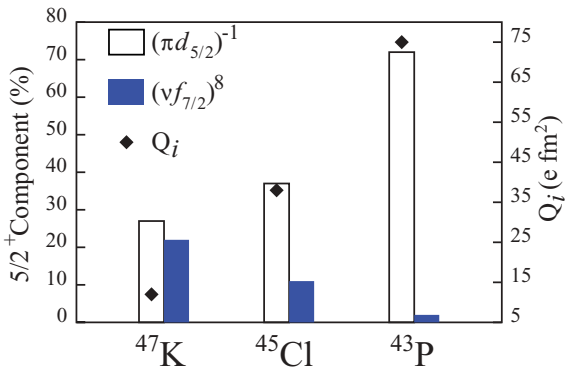

FIG. 5. (Color online) Left axis: Contribution, in %, of the $(\pi d_{5/2})^{-1}$ $[(\nu f_{7/2})^8]$ component to the proton (neutron) wave function of the $5/2^+$ states displayed as black levels in Fig. 4. Right axis: Intrinsic quadrupole moment, Q_i, associated with diamond symbol, for the $5/2^+$ state displayed as black levels in Fig. 4. $Q_i$is calculated assuming a K value of $K = 5/2$.

the well-bound $\pi d_{5/2}$ orbit. The remaining part of the wave function corresponds to coupled proton-neutron components, accounting for the rather small $(\nu f_{7/2})^8$ contribution to the neutron wave function in the corresponding state (see Fig. 5). Here we would like to point out that Fig. 5 presents only a fraction of interest of the proton and neutron WFs for the $5/2^+$ states built on the $\pi d_{5/2}$ orbit. The reported proton (neutron) components are obtained by summing over all neutron (proton) configurations associated with the $(\pi d_{5/2})^{-1}$ proton component [$(\nu f_{7/2})^8$ neutron component] in the WFs of the $5/2^+$ states considered. For example, a pure state consisting only of the $(\pi d_{5/2})^{-1}$-$(\nu f_{7/2})^8$ configuration would decompose into a $(\pi d_{5/2})^{-1}$ proton component of 100% and a $(\nu f_{7/2})^8$ neutron component of 100%.

In the more exotic ${}^{45}_{17}$Cl nucleus, the aforementioned quasidegeneracy of $1/2^+$ and $3/2^+$ states is also observed below 200 keV. The main component of the proton wave function of the $5/2^+_1$ calculated at 1 MeV corresponds to the coupling of a proton hole in the $\pi s_{1/2}$ or $\pi d_{3/2}$ orbit to the 2^+_1 state of the core nucleus ^{46}Ar (reported as a diamond symbol in the level scheme of ${}^{45}_{17}$Cl). The $5/2^+_2$ state at 1.6 MeV is the first one calculated with a non-negligible contribution, 35%, arising from the $\pi d_{5/2}$ orbit as seen from Fig. 5. Each of the calculated levels presented in Fig. 4 for ${}^{45}_{17}$Cl has an experimental counterpart [10,38]. It is striking to note the drop by about 3 MeV of the $5/2^+$ state of interest in between ${}^{47}_{19}$K and ${}^{45}_{17}$Cl. This drop is associated with an increased contribution from the $\pi d_{5/2}$ proton orbit to the wave function of the state and a decreased contribution from the natural $(\nu f_{7/2})^8$ neutron configuration (see Fig. 5). About 35% (30%) of the neutron wave function corresponds to the $(\nu f_{7/2})^{-1}r^1$ $[(\nu f_{7/2})^{-2}r^2]$ intruder configuration. Here r refers to one of the $\nu p_{3/2}$, $\nu p_{1/2}$ or $\nu f_{5/2}$ neutron orbits. A decomposition of the total energy of the states of interest in terms of monopole and multipole contributions similar to that discussed in the previous section has been performed in $N = 28$ isotones. It is instructive to know that in ${}^{47}_{19}$K, multipole contributions (MuC) do not significantly favor any of the calculated states. On the contrary, in ${}^{45}_{17}$Cl, the multipole energy contributions for the $1/2^+$, $3/2^+$, and $5/2^+_1$ states are -11.9, -10.1, and -11.2 MeV, respectively, while amounting to -13.1 MeV for the $5/2^+_2$ state.

As seen from Fig. 4, the decrease in energy of the $5/2^+$ state built on the $\pi d_{5/2}$ orbit continues further in ${}^{43}_{15}$P, a $5/2^+_1$ state lying as low as 970 keV in agreement with recent data [14]. Figure 5 shows the negligible contribution of the natural neutron configuration, $(\nu f_{7/2})^8$, to the wave function of the $5/1^+_1$ state in ${}^{43}_{15}$P, while the contribution from the $(\pi d_{5/2})^{-1}$ proton configuration reaches about 70%.

A striking difference between ${}^{43}_{15}$P and ${}^{47}_{19}$K or ${}^{45}_{17}$Cl is the prediction of a deformed sequence built on top of the $5/2^+_1$ level in ${}^{43}_{15}$P. No such sequence is found neither for ${}^{47}_{19}$K nor for ${}^{45}_{17}$Cl. The right axis in Fig. 5 is associated with the set of black diamond symbols representing the intrinsic quadrupole moments, Q_i, of the $5/2^+$ states of interest in the present discussion. These quadrupole moments have been estimated assuming a $K = 5/2$ value (K being the projection of the total angular momentum J onto the z axis of the intrinsic system) for the corresponding states. It is clearly seen that

TABLE II. Spectroscopic properties of the states belonging to the deformed sequence in $^{43}_{15}$P: intrinsic quadrupole moments, Q_i in e fm^2 (calculated assuming a K value of $K = 5/2$); mean occupation numbers of the $\pi d_{5/2}$ proton orbit, $n_\pi(d_{5/2})$; contribution of the $(\nu f_{7/2})^8$ and $(\nu f_{7/2})^{-2}$ components, in percent, to the neutron wave function; and monopole/multipole contributions to the total energy of the state, MoC/MuC in MeV.

	$5/2^+$	$7/2^+$	$9/2^+$	$11/2^+$
Q_i	75	100	16	55
$n_\pi(d_{5/2})$	4.74	4.79	4.89	4.78
$(\nu f_{7/2})^8$	2	1	2	0
$(\nu f_{7/2})^{-2}$	63	60	49	57
MoC	−214.9	−215.4	−216.4	−215.0
MuC	−19.9	−18.7	−17.0	−17.3

deformation of the $5/2^+$ states increases along the $N = 28$ isotonic chain. Consistently, the increasing deformation can be associated with the aforementioned increase (decrease) of the $(\pi d_{5/2})^{-1}$ proton contribution [natural $(\nu f_{7/2})^8$ neutron contribution] to the WF of the states. The deformed sequence states calculated in ^{43}P ($7/2^+$, $9/2^+$, and $11/2^+$ states) are shown in Fig. 4. In this scheme a state of spin J mainly decays via the $M1$ transition toward the state of spin $J - 1$ and via the $E2$ transition toward the state of spin $J - 2$, as shown in Fig. 4. The $E2$ transition rates associated with the $J \to J - 1$ transitions are calculated to be about 10 times smaller than the corresponding $M1$ transition rates. The $5/2^+_1$ sequence head decays to the $1/2^+_1$ state via a weak $E2$ transition [$B(E2, 5/2^+_1 \to 1/2^+_1) = 7\, e^2$ fm^4] and toward the $3/2^+_1$ state via an $M1$ transition [$B(M1, 5/2^+_1 \to 3/2^+_1) = 0.017\ \mu_N^2$].

Table II summarizes some properties for the states involved in the deformed sequence, such as their intrinsic quadrupole moment, Q_i. The reported $Q_i$values clearly show: (i) the prolate deformation associated with the sequence, and (ii) the strong variation in deformation with growing excitation energy along the sequence. From the latter observation it appears that the sequence cannot be regarded as a rotational band. For this reason, in the following, the term *deformed sequence* (DS) will continue to be used. As mentioned previously for the $5/2^+_1$ state and as seen from Table II, the states of the DS have: (i) a similar proton wave function with the main configuration corresponding to a single proton hole in the $\pi d_{5/2}$ orbit, as reflected by the mean occupation number of the $\pi d_{5/2}$ orbit; (ii) a similar neutron wave function corresponding to the intruder configuration $(\nu f_{7/2})^{-2} r^2$; and (iii) a negligible contribution from the natural neutron configuration $[(\nu f_{7/2})^8]$.

Neglecting correlations (i.e., multipole contribution to the total energy of the considered states) in $^{43}_{15}$P, the GS of the nucleus is the $3/2^+_1$ state (Fig. 4) with a monopole contribution to the total energy of the state of −220.9 MeV. As seen from Table II the monopole contributions to the total energy of the DS's states are all around the same value (-215.6 ± 0.7 MeV), about 5 MeV higher than that of the corresponding $3/2^+$ monopole ground state. However once correlations are considered (see Table II), the states belonging to the DS are energetically favored, the $5/2^+$ sequence head lying only 1 MeV above the $1/2^+$-$3/2^+$ doublet. We mention that the intruder neutron configuration is not specifically associated with the $(\pi d_{5/2})^{-1}$ proton configuration. Indeed the $(\nu f_{7/2})^{-2} r^2$ configuration contributes to a level of about 45% to the wave function of the $1/2^+_1$ and $3/2^+_1$ states in $^{43}_{15}$P.

The present discussion demonstrates the increasing role of proton excitations across the $Z = 14$ gap in exotic nuclei along the $N = 28$ shell closure. Consistently with the results obtained for $N = 27$ isotones, correlations are found to gradually increase as a function of N/Z at $N = 28$. Associated with the increasing correlations, the $(\pi d_{5/2})^{-1}$ component in the proton wave function of the $5/2^+$ states becomes dominant. From $^{47}_{19}$K down to $^{43}_{15}$P, the excitation energy of the studied $5/2^+$ state is drastically lowered by about 4 MeV. In $^{43}_{15}$P, a deformed prolate sequence is calculated on top of the $5/2^+_1$ state and the intruder nature of the neutron configuration of the states is found.

C. $N = 29$ isotones

The structure of neutron-rich $N = 29$ isotones has not been discussed much in the literature. This is probably related to the lack of experimental data for these isotones that are difficult to produce. In the following the structure of these isotones is studied from $Z = 20$ down to $Z = 15$. Nuclei with lower Z values are very weakly bound and their calculated structure might not be well accounted for by the present SM approach. Even-odd and odd-odd isotones are discussed separately.

The structure of $N = 29$ isotones is expected to resemble that of $N = 27$ isotones since the former consist of one particle and the latter of one hole on top of $N = 28$. However, the separation in excitation energy between the states built on the $\nu f_{7/2}$ and $\nu p_{3/2}$ orbitals (forming the $N = 28$ gap) differs by about 1 MeV between $N = 27$ and $N = 29$ isotones, as seen in the following section. For later convenience the origin of this difference is pointed out here for Ca isotopes based on simplistic SM arguments. As a first approximation the $7/2^-$ GS in $^{47}_{20}$Ca$_{27}$ can be considered to be built on the $(\nu f_{7/2})^{-1}$ neutron configuration, and the $3/2^-_1$ state results from the excitation of a single neutron from the $\nu f_{7/2}$ orbit to the $\nu p_{3/2}$ one leading to the $(\nu f_{7/2})^{-2}$ $(\nu p_{3/2})^1$ neutron configuration. Similarly, in $^{49}_{20}$Ca$_{29}$ the configuration of the WF of the $3/2^-$ GS is $(\nu f_{7/2})^8$ $(\nu p_{3/2})^1$ and the configuration of the $7/2^-_1$ excitation is $(\nu f_{7/2})^{-1}$ $(\nu p_{3/2})^2$. In these dominant configurations, pairs of neutron holes in the $\nu f_{7/2}$ orbit and neutron particles in the $\nu p_{3/2}$ orbit are mainly coupled to $J = 0$ and $T = 1$. The difference in the $3/2^-_1$-$7/2^-_1$ energy splitting between ^{47}Ca and ^{49}Ca, Δ, can be expressed as a function of its monopole and multipole contributions: $\Delta = \Delta_m + \Delta_M$. Neglecting the mass dependency of the matrix elements between $A = 47$ and $A = 49$, one finds from the simple SM configurations introduced previously that $\Delta_m = V^{T=1}_{f_{7/2}, f_{7/2}} - V^{T=1}_{p_{3/2}, p_{3/2}} \simeq -0.1$ MeV, where $V^{T=1}_{i,i}$ is the $T = 1$ monopole centroid for the orbit i. Thus the monopole contribution to Δ is minor; that is, Δ is mainly a multipole effect, most of which is due to the difference between the $\nu f_{7/2}$ and $\nu p_{3/2}$ pairing matrix elements. Neglecting other contributions to Δ_M, one estimates $\Delta \simeq 1.1$ MeV.

1. Even-odd isotones

The present discussion aims at investigating if and how correlations, systematically observed or predicted in neutron-rich nuclei at $N = 27$ and 28, impact the structure of even-odd $N = 29$ isotones. $N = 29$ isotones are expected to have low-lying states built on the $(\nu f_{7/2})^8 r^1$ neutron configuration. Here r stands for one of the $\nu p_{3/2}$, $\nu p_{1/2}$, or $\nu f_{5/2}$ neutron orbits. In $^{49}_{20}$Ca, only small fragmentation of the spectroscopic strength corresponding to the r orbits is experimentally observed [45,46]. No $7/2^-$ state built on the $\nu f_{7/2}$ neutron orbit with significant neutron spectroscopic factor has been reported. It shows that the $\nu f_{7/2}$ orbit is to a large extent fully occupied in the ground state of $^{48}_{20}$Ca, thus hindering neutron transfer to this orbit via (d, p) or similar one neutron transfer reactions. The first $7/2^-$ state is calculated at 3.1 MeV above the $3/2^-$ GS of $^{49}_{20}$Ca. The excitation energy difference between the $3/2^-_1$ and $7/2^-_1$ states is 1 MeV higher in $^{49}_{20}$Ca as compared to its value in $^{47}_{20}$Ca, in agreement with the previously estimated value of Δ.

Below $Z = 20$, to the best of our knowledge, spectroscopic information on even-odd $N = 29$ isotones is restricted to $^{47}_{18}$Ar [12,47]. In this nucleus, like for $^{49}_{20}$Ca, large spectroscopic factors are reported for the $3/2^-$ GS and the low-lying $1/2^-_1$ state (at 1.3 MeV), pointing toward a single-particle nature [12]. Contrary to $^{49}_{20}$Ca, a low-lying $7/2^-$ state (lying at about 1.8 MeV) has been reported with a non-negligible neutron spectroscopic factor, pointing toward the reduction of the $N = 28$ shell closure at $Z = 18$ [12]. Supporting this conclusion is the observation of a low-lying $5/2^-$ state, observed at 1.23 keV, interpreted as arising from the coupling of a $\nu p_{3/2}$ neutron to the 2^+ core excitation [47]. Hence, already at $Z = 18$, experimental data and their SM interpretation suggest a moderate onset of correlations.

Further away from the stability line, in $^{45}_{16}$S, no experimental data exist. The low-lying $1/2^-_1$, $3/2^-_1$, and $7/2^-_1$ states have been calculated within the present SM approach. Some spectroscopic properties of these states are given in Table III. As seen from the table, the level scheme calculated for $^{45}_{16}$S is slightly compressed as compared to that for $^{47}_{18}$Ar. In particular, the $7/2^-_1$ state lies about twice lower in excitation energy in $^{45}_{16}$S than in $^{47}_{18}$Ar. Like for $^{47}_{18}$Ar, the non-negligible neutron spectroscopic factor calculated for the $7/2^-$ state in $^{45}_{16}$S (see Table III) is a strong indication that the $N = 28$ shell closure is no longer effective in the core nucleus. This remark is consistent with previous experimental and theoretical studies on $^{44}_{16}$S pointing to shape coexistence [17,23,28,30]. The rather large spectroscopic factors associated with the $1/2^-$ and $3/2^-$ states indicate their dominant single-particle nature.

TABLE III. Calculated excitation energies (E), in MeV; neutron spectroscopic factors (C^2S) corresponding to (d, p) transfer reaction on the $N = 28$ core nucleus in its ground state; multipole contribution (MuC), in MeV; and spectroscopic quadrupole moments (Q_s), in e fm^2, for the states of interest in ^{45}S, labeled by their spin/parity, J^π.

J^π	E	C^2S	MuC	Q_s
$3/2^-_1$	GS	0.46	−13.3	−9
$1/2^-_1$	0.63	0.54	−14.5	
$7/2^-_1$	0.74	0.12	−14.8	29

As seen from Table III, the multipole contributions to the total energy of the states of interest do not differ from those reported for $N = 27$ and 28 isotones. It suggests the presence of correlations as in $^{44}_{16}S_{28}$ and $^{43}_{16}S_{27}$. Hence deformation might be expected for $^{45}_{16}$S, as supported by the spectroscopic quadrupole moments reported in Table III, especially that for the $7/2^-_1$ state. Other excited states are calculated in $^{45}_{16}$S but not reported in Table III because of their too low binding energies. Particularly interesting is a group of $9/2^-$, $11/2^-$, and $13/2^-$ states calculated at 1.85, 2.79, and 4.18 MeV, respectively, that might be viewed together with the $7/2^-_1$ state as a deformed structure. Indeed, these states are linked by strong $M1$ and $E2$ transitions, following the same decay pattern as that reported for $^{43}_{15}$P in Fig. 4, with typical transition probabilities of $B(M1) \simeq 0.15\ \mu_N^2$ and $B(E2) \simeq 40\ e^2$ fm^4. These states present the same intrinsic neutron configuration $[(\nu f_{7/2})^{-1}(\nu p_{3/2})^{+2}]$ suggesting a $K = 7/2$ value for the $7/2^-_1$ state reported in Table III. An axial deformation parameter value, $\beta \simeq 0.3$, might thus be deduced for the $7/2^-_1$ state. No clear signatures for deformed structures are found on top of the $1/2^-_1$ and $3/2^-_1$ states. This foretells a moderate deformation for these latter states as compared to that for the $7/2^-_1$ state, which is consistent with the rather small spectroscopic quadrupole moment reported in Table III for the $3/2^-_1$ state. One notices that similar arguments for $^{47}_{18}$Ar lead to rather spherical shapes for the states discussed for that nucleus.

The present discussion shows that correlations impact on the structure of even-odd $N = 29$ isotones as on other studied isotones. Correlations are not developed enough at $Z = 18$ to imply large deformation in $^{47}_{18}$Ar; however, they lower the intruder neutron configuration built on the $\nu f_{7/2}$ orbit as compared to $Z = 20$. In $^{45}_{16}$S, this intruder configuration lies at low excitation energy and is associated with a well-deformed prolate shape. This intruder configuration coexists with the natural one built on the $\nu p_{3/2}$ orbit and associated with a rather spherical shape.

2. Odd-odd isotones

This section is devoted to the structure of the low-lying states in $^{48}_{19}$K, $^{46}_{17}$Cl, and $^{44}_{15}$P $N = 29$ isotones. As already discussed for odd-odd $N = 27$ isotones, the low-lying states of interest for these nuclei are built on the $\pi d_{3/2}$-$\nu f_{7/2}$ and $\pi d_{3/2}$-$\nu p_{3/2}$ configurations.

The $\pi d_{3/2}$ and $\pi s_{1/2}$ proton orbits being quasidegenerate in the studied mass region, non-negligible mixing is expected in the wave functions of the states of these multiplets. As compared to odd-odd $N = 27$ isotones, states built on the $\pi d_{3/2}$-$\nu p_{3/2}$ configuration [i.e., the $(0,1,2,3)^-$ states] are expected to be lower in excitation energy than those built on the $\pi d_{3/2}$-$\nu f_{7/2}$ configuration [i.e., the $(2,3,4,5)^-$ states] in $N = 29$ isotones. Figure 6 presents the level schemes calculated for the aforementioned odd-odd $N = 29$ isotones, restricted to the states of interest here, and confirms the aforementioned expectation. As seen from this figure, two 1^- and 2^- states are reported as being part of the $\pi d_{3/2}$-$\nu p_{3/2}$ multiplet. The degeneracy of these states arises from the corresponding

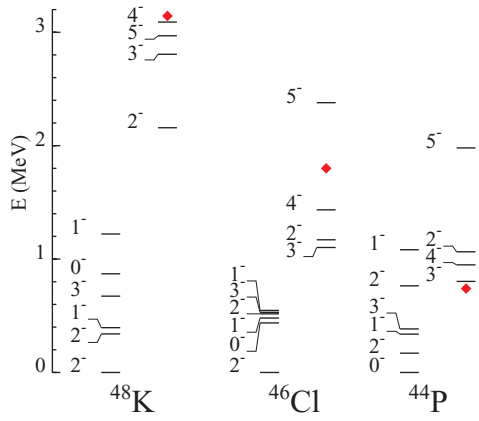

FIG. 6. (Color online) Calculated level schemes in odd-odd $N = 29$ isotones of interest. States originating from the $\pi d_{3/2}$-$\nu f_{7/2}$ and $\pi d_{3/2}$-$\nu p_{3/2}$ couplings are shown. States clearly identified as being built on the $\nu p_{3/2}$ orbit are shifted on the left part of the level scheme for each isotone. The diamond symbol indicates, for each ${}^{A}_{Z}X$ isotone, the position of the first $7/2^-_1$ state in the core ${}^{A+1}_{Z+1}Y$ nucleus.

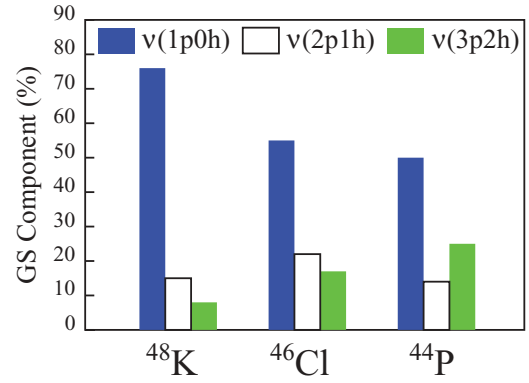

FIG. 7. (Color online) Components of (1p0h), (2p1h), and (2p3h) neutron configurations in the ground-state wave function of odd-odd $N = 29$ isotones.

degeneracy of the $\pi s_{1/2}$ and $\pi d_{3/2}$ orbitals. For example, in ${}^{48}_{19}$K, 70% of the wave function of the 2^-_1 state corresponds to the $(\pi s_{1/2})^1(\pi d_{3/2})^4$-$(\nu f_{7/2})^8(\nu p_{3/2})^1$ configuration, while 70% of the wave function of the 2^-_2 state corresponds to the $(\pi s_{1/2})^2(\pi d_{3/2})^3$-$(\nu f_{7/2})^8(\nu p_{3/2})^1$ configuration. Configuration mixing is even more apparent when considering the wave functions of the 1^- states. Indeed two main components are present in the wave function of the 1^-_1 state: (i) 52% for the $(\pi s_{1/2})^2(\pi d_{3/2})^3$-$(\nu f_{7/2})^8(\nu p_{3/2})^1$ configuration, and (ii) 15% for the $(\pi s_{1/2})^1(\pi d_{3/2})^4$-$(\nu f_{7/2})^8(\nu p_{3/2})^1$ configuration. Main configurations are the same for the wave function of the 1^-_2 state, but the percentages are reversed. Similar mixing between the $\pi d_{3/2}$-$\nu f_{7/2}$ and $\pi s_{1/2}$-$\nu f_{7/2}$ configurations are observed for the 3^- and 4^- states of the second multiplet of interest here. As mentioned earlier, the consequence of the degeneracy of the $\pi s_{1/2}$ and $\pi d_{3/2}$ orbitals has been discussed elsewhere and will not be further addressed here.

In ${}^{48}_{19}$K, states built on the $\nu f_{7/2}$ neutron orbit (reported in the right part of the corresponding level scheme in Fig. 6) lie at an excitation energy in agreement with that for the $7/2^-_1$ state calculated in ${}^{49}_{20}$Ca (diamond symbol in the level scheme of ${}^{48}_{19}$K). States of interest in ${}^{48}_{19}$K have rather pure neutron wave functions for which about 70% corresponds to the $(\nu f_{7/2})^8(\nu p_{3/2})^1$ (i.e., 1p0h, where particle and hole are counted with respect to the $\nu f_{7/2}$ orbit) configuration or to the $(\nu f_{7/2})^{-1}(\nu p_{3/2})^2$ (i.e., 2p1h) configuration, depending on the considered multiplet. This is exemplified in Fig. 7 for the GS wave function where configurations corresponding to one or two holes in the $\nu f_{7/2}$ orbit are seen to contribute at a level of 20% only.

The discussion reported in Sec. II C1 showed that the excitation energy of the $7/2^-_1$ state in even-odd $N = 29$ isotones decreases while N/Z increases. The corresponding excitation energies are indicated as diamond symbols in Fig. 6. Consistently, in odd-odd $N = 29$ isotones, the excitation energy of the states belonging to the multiplet built on the $\nu f_{7/2}$ orbit decreases from about 3 MeV in ${}^{48}_{19}$K down to about 1 MeV in ${}^{44}_{15}$P (see Fig. 6). This decrease goes in concert with the increase in configuration mixing in the wave function of the states of interest, as seen for the particular case of the GS wave functions in Fig. 7. From ${}^{48}_{19}$K to ${}^{44}_{15}$P the contribution of the natural neutron configuration (i.e., 1p0h) expected for the GS wave function decreases from about 75% down to about 50% in favor of the contribution of the intruder neutron configurations (i.e., either 2p1h or 3p2h) that increases from about 20% up to 40%. This evolution in the natural/intruder balance in the considered wave functions is a consequence of the increase in correlation energy along the $N = 29$ isotonic chain. For the isotones of interest multipole energy contribution to the total energy of the considered states is of similar amplitude as for odd-odd $N = 27$ isotones (see Table I).

The previous discussion ascertains the conclusions from Sec. II C1: correlations impact on $N = 29$ as on other studied isotones. Configuration mixing in the wave functions of the low-lying states of interest increases with N/Z as does multipole energy contribution. It is interesting to realize that the decrease in excitation energy of the intruder configuration from $Z = 19$ down to $Z = 15$ is equivalent in $N = 29$ and $N = 27$ isotones. The inversion between natural and intruder configurations reported for $N = 27$ isotones is not found at $N = 29$ mainly because of the difference in the $\nu f_{7/2}$ and $\nu p_{3/2}$ pairing matrix elements.

III. CONCLUDING REMARKS

From the present shell model study of $N = 27$, $N = 28$, and $N = 29$ isotones a consistent picture emerges of the evolution of the nuclear structure in this mass region. The $N = 28$ shell closure is reduced while moving away from the valley of stability. This reduction is modest. Experimentally, it amounts to about 330 keV per pair of protons removed from the *sd* shell [12]. Both shell model [30] and mean field [23] calculations are in agreement on the amplitude of this reduction. Hence, with a starting value of about 4.8 MeV at $Z = 20$, the $N = 28$ shell gap is predicted to be about 3.8 MeV in silicon isotopes.

While the $N = 28$ shell gap is gradually reduced with increasing N/Z ratio, correlations strongly increase. The

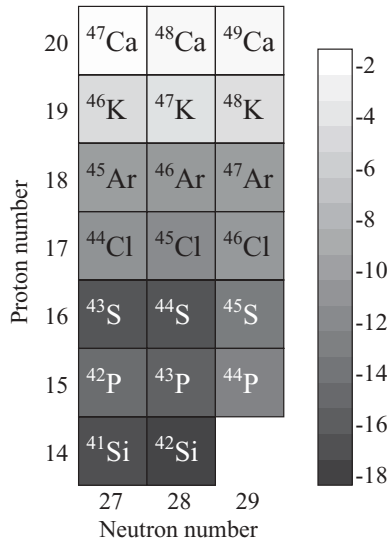

FIG. 8. Portion of the nuclear chart studied in the present work. The gray scale represents the amount of correlation energy, in MeV, in the ground state of the considered nuclei.

amount of correlation energy in the studied mass region is mainly independent on the neutron number of the nuclei. This point is exemplified in Fig. 8 displaying the multipole contribution to the total energy of the ground states of $N =$ 27–29 nuclei. This figure summarizes one result of the present work: Adding neutrons from $N = 27$ up to $N = 29$ does not significantly modify correlation energy at a fixed proton number, while removing protons at a fixed neutron number implies an important increase in correlation energy. This feature shows that protons play a key role in the development of collectivity around $N = 28$. It is to be noted that the increase in correlation energy is by far much larger than the reduction of the $N = 28$ gap along the studied isotonic chains.

For each studied isotonic chain, configuration mixing increases with correlations giving rise to a decrease by about 2–2.5 MeV of neutron intruder configurations from $Z = 20$ down to $Z = 14$. At $N = 27$ and $N = 28$, neutron intruder configurations become the ground-state ones as soon as $Z < 17$. Correlations also affect the proton part of the wave functions of the studied isotones. It has been shown for odd-even $N = 28$ isotones where a gradual lowering of the states built on the $\pi d_{5/2}$ orbit between $Z = 19$ and $Z = 15$ is found. In $^{43}_{15}P_{28}$ a deformed prolate sequence built on the $\pi d_{5/2}$ proton orbit is predicted.

Consistently with the previous results, the nuclear shapes of studied isotones also gradually evolve with the N/Z ratio. At $Z = 20$, correlations are not developed and these nuclei present spherical shapes. Configuration mixing is appreciable for $Z = 18$ nuclei that present a slight prolate deformation. At $Z = 16$, coexistence of rather spherical and well-deformed prolate shapes ($\beta \simeq 0.3$) is predicted for each studied isotonic chain (see Refs. [19,30] for isotopes not specifically discussed in the present work), while $^{42}_{14}$Si is predicted to be a well-deformed oblate rotor [30]. These shell model results agree with conclusions drawn from mean field calculations [23]. Moreover, within the mean field framework, shape evolution in $N = 28$ isotones is found to be mainly driven by deformed proton shell effects [23], in agreement with present conclusions.

Perspectives of the present work consist of experimental suggestions. At $N = 27$, it would be interesting to study the intruder nature of the $^{42}_{15}P_{27}$ ground state. Even if not specifically discussed in the present work, it would also be compelling to identify the states belonging to the predicted rotational band in $^{43}_{16}S_{27}$ [19] to ascertain the present description of nuclear structure in this mass region. At $N = 28$, confirmation of the key role of proton excitations in driving the structure of exotic nuclei in this mass region could be achieved through the study of the predicted deformed sequence in $^{43}_{15}P_{28}$. At $N = 29$, even if challenging, it would be of interest to quantify the deformation of the $7/2^-_1$ intruder state in $^{45}_{16}S_{29}$. Further study of the neutron spectroscopic factors in this nucleus would provide valuable information.

ACKNOWLEDGMENTS

It is a pleasure to thank A. Navin, F. Nowacki, S. Péru, N. Pillet, and M. Rejmund for critical reading of the manuscript and enlightening discussions.

[1] O. Sorlin *et al.*, Phys. Rev. C **47**, 2941 (1993).
[2] H. Scheit *et al.*, Phys. Rev. Lett. **77**, 3967 (1996).
[3] T. Glasmacher *et al.*, Phys. Lett. B **395**, 163 (1997).
[4] R. W. Ibbotson *et al.*, Phys. Rev. Lett. **80**, 2081 (1998).
[5] R. W. Ibbotson, T. Glasmacher, P. F. Mantica, and H. Scheit, Phys. Rev. C **59**, 642 (1999).
[6] F. Sarazin *et al.*, Phys. Rev. Lett. **84**, 5062 (2000).
[7] B. Jurado *et al.*, Phys. Lett. B **649**, 43 (2007).
[8] D. Sohler *et al.*, Phys. Rev. C **66**, 054302 (2002).
[9] Zs. Dombrádi *et al.*, Nucl. Phys. A **727**, 195 (2003).
[10] O. Sorlin *et al.*, Eur. J. Phys. A **22**, 173 (2004).
[11] A. Gade *et al.*, Phys. Rev. C **71**, 051301(R) (2005).
[12] L. Gaudefroy *et al.*, Phys. Rev. Lett. **97**, 092501 (2006).
[13] L. Gaudefroy *et al.*, Phys. Rev. C **78**, 034307 (2008).
[14] L. A. Riley *et al.*, Phys. Rev. C **78**, 011303(R) (2008).
[15] L. A. Riley *et al.*, Phys. Rev. C **79**, 051303(R) (2009).
[16] L. A. Riley *et al.*, Phys. Rev. C **80**, 037305 (2009).
[17] S. Grévy *et al.*, Eur. Phys. J. A **25**, 111 (2005).
[18] B. Bastin *et al.*, Phys. Rev. Lett. **99**, 022503 (2007).
[19] L. Gaudefroy *et al.*, Phys. Rev. Lett. **102**, 092501 (2009).
[20] D. Hirata, K. Sumiyoshi, B. V. Carlson, H. Toki, and I. Tanihata, Nucl. Phys. A **609**, 131 (1996).
[21] T. R. Werner *et al.*, Nucl. Phys. A **597**, 327 (1996).
[22] G. A. Lalazissis, D. Vretenar, P. Ring, M. Stoitsov, and L. M. Robledo, Phys. Rev. C **60**, 014310 (1999).
[23] S. Péru, M. Girod, and J. F. Berger, Eur. Phys. J. A **9**, 35 (2000).
[24] R. Rodríguez-Guzmán, J. L. Egido, and L. M. Robledo, Phys. Rev. C **65**, 024304 (2002).
[25] J. Retamosa, E. Caurier, F. Nowacki, and A. Poves, Phys. Rev. C **55**, 1266 (1997).

[26] D. J. Dean, M. T. Ressell, M. Hjorth-Jensen, S. E. Koonin, K. Langanke, and A. P. Zuker, Phys. Rev. C **59**, 2474 (1999).
[27] E. Caurier, F. Nowacki, and A. Poves, Eur. Phys. J. A **15**, 145 (2002).
[28] E. Caurier, F. Nowacki, and A. Poves, Nucl. Phys. A **742**, 14 (2004).
[29] E. Caurier, G. Martínez-Pinedo, F. Nowacki, A. Poves, and A. P. Zuker, Rev. Mod. Phys. **77**, 427 (2005).
[30] F. Nowacki and A. Poves, Phys. Rev. C **79**, 014310 (2009).
[31] E. Caurier, ANTOINE code, IReS, Strasbourg 1989–2002.
[32] E. Caurier and F. Nowacki, Acta Phys. Pol. B **30**, 705 (1999).
[33] M. Dufour and A. P. Zuker, Phys. Rev. C **54**, 1641 (1996).
[34] M. De Rydt *et al.*, Phys. Rev. C **81**, 034308 (2010).
[35] W. W. Deahnick, J. H. Orloff, T. Canada, and T. S. Bhatia, Phys. Rev. C **10**, 136 (1974).
[36] S. Angelo, A. A. Pilt, and J. A. Kuehner, Phys. Rev. C **22**, 427 (1980).
[37] P. D. Cottle and K. W. Kemper, Phys. Rev. C **58**, 3761 (1998).
[38] A. Gade *et al.*, Phys. Rev. C **74**, 034322 (2006).
[39] O. Sorlin and M.-G. Porquet, Prog. Part. Nucl. Phys. **61**, 602 (2008).
[40] P. D. Cottle and K. W. Kemper, Phys. Rev. C **66**, 061301(R) (2002).
[41] C. M. Campbell *et al.*, Phys. Rev. Lett. **97**, 112501 (2006).
[42] J. Fridmann *et al.*, Phys. Rev. C **74**, 034313 (2006).
[43] C. M. Campbell *et al.*, Phys. Lett. B **652**, 169 (2007).
[44] P. Doll, G. J. Wagner, and K. T. Knöpfle, Nucl. Phys. A **263**, 210 (1976).
[45] R. Abegg *et al.*, Nucl. Phys. A **303**, 121 (1978).
[46] Y. Uozumi *et al.*, Nucl. Phys. A **576**, 123 (1994).
[47] S. Bhattacharyya *et al.*, Phys. Rev. Lett. **101**, 032501 (2008).